



Seasonal distribution of cirrus cloud characteristics and their rapid descent from polarization lidar measurements at the west coast of India

M. A. Aswini^{1,2} · R. D. Ruchith¹ · Subrata Kumar Das³ · V. Ramaswamy¹ · P. M. Muraleedharan¹ · Ashwini Kumar¹

Received: 28 March 2022 / Accepted: 29 May 2023 / Published online: 12 July 2023

© The Author(s), under exclusive licence to Springer-Verlag GmbH Austria, part of Springer Nature 2023

Abstract

Cirrus clouds are highly reflective clouds that play an important role in the atmospheric radiative balance and contribute to climate change. We present the seasonal distribution of cirrus cloud occurrence, characteristics and evolution over a coastal station (Goa, 15.4°N, 73.8°E, 40 m above MSL) in India using ground-based micro pulse lidar and radiosonde observations from July 2013 to June 2015. The frequency of cirrus occurrence was approximately 44%, 33%, 17% and 6% in winter (JF), premonsoon (MAM), southwest monsoon (JJAS) and postmonsoon season (OND), respectively. Thicker cirrus was more frequent in September, with an average value of $> 1.7 \pm 0.89$ km. The frequency of cirrus descent occurs almost similarly in monsoon and postmonsoon (42% and 43% respectively). Two extreme cirrus descending cases were observed during the monsoon: (1) on 22 August 2014 with a displacement of 9.6 km from the initial height of 14 km with a descending rate and geometrical thickness of 0.4 ms^{-1} and 1.5 km, respectively, and (2) on 14 September 2013 with a displacement of 7.8 km with descending rate and thickness of 0.2 ms^{-1} and 2.3 km respectively. Relatively high humidity ($> 60\%$) and low (< -20 °C) ambient temperature caused thick cirrus formation in September 2013. However, during August 2014 event, relatively thinner cirrus was observed, and the same is attributed to lower humidity conditions (45 to 60%). The wind shear associated with the tropical easterly jet (TEJ) plays a major role in cirrus displacement by modifying their vertical velocity. The positive and negative vertical velocity fields cause cirrus to have a descending shape. The gradual descending pattern of cirrus is moving parallel to the vertical velocity contour, while the rapid descending in 2014 was mainly due to the occurrence of cirrus perpendicular to the velocity contour. Overall, this study highlights the descending nature of cirrus clouds over a coastal station in India, which can impact surface radiative characteristics.

1 Introduction

Cirrus clouds are high-altitude thin, wispy clouds that cover almost 20–50% of the Earth's atmosphere (Veerabuthiran 2004; Liou 1986; Lynch 2000; Stubenrauch et al. 2013). Owing to their interaction with incoming solar radiation, they have the potential to modulate the Earth's radiation budget (Choi and Ho 2006; Podglajen et al. 2015; Hansen et al. 1997; Chen,

et al. 2000; Hartmann et al. 1992; Burkhardt and Kärcher 2011; Takano and Liou 1995; Zeng et al. 2021; Campbell et al. 2021) and can influence the weather and climate (Baran 2012; Muri et al. 2014; Heidinger et al. 2015; Kärcher 2018; Lawson et al. 2019). The macro- and microphysical properties of cirrus determine the cooling or warming effect (Noel et al. 2006; Stubenrauch, et al. 2010). The cirrus clouds are mainly composed of ice crystals. However, they are occasionally enriched with supercooled water droplets (Krämer et al. 2009; Jeffery and Austin 1997). Cirrus cloud formation occurs at typical temperatures of less than -20 °C (Liou 1986; Jensen et al. 2001; Korolev and Isaac 2006; Koop et al. 2000), and the shape and size of ice crystals within these clouds depend on the ambient temperature and relative humidity (Liou 2002). In general, cirrus cloud's genesis can be explained either via deep convective activity or due to the nucleation of the ice crystals near the tropopause (Veerabuthiran 2004). Cirrus cloud's typical lifetime varies from a few hours to days (Taylor et al.

✉ Ashwini Kumar
ashwinik@nio.org

¹ Geological Oceanography Division, CSIR-National Institute of Oceanography, Dona Paula, Panaji, Goa 403004, India

² Bharathidasan University, Tiruchirappalli 620024, Tamil Nadu, India

³ Ministry of Earth Sciences, Indian Institute of Tropical Meteorology, Pashan, Pune 411008, India

2011; Meenu et al. 2011). The interaction with incoming solar radiation, which includes reflection, absorption and transmission, depends on the coverage, position, thickness and size distribution of ice crystals (Liou 1986; Baran 2009; Heidinger et al. 2015), which eventually determine their role in impacting the climate. In the tropical tropopause layer, the optically thin cirrus clouds have a low albedo which causes positive radiative forcing and the greenhouse effect, which warms the atmosphere. Optically thick cirrus clouds have high albedo, which produces negative radiative forcing, and the albedo effect cools the atmosphere (Jensen et al. 1994; McFarquhar et al. 2000; Fu and Liou 1993; Fahey and Schumann 1999). The degree and extent of greenhouse or albedo effects will lead to significant atmospheric differential heating and cooling on vertical as well as horizontal scales and appear to have a profound influence on synoptic and regional weather systems (Liou 1986; Forster et al. 2007; Campa et al. 2008). For well-mixed greenhouse gases, a positive radiative forcing implies global warming (Ramanathan and Collins 1991; Hansen et al. 1997). However, cirrus induces a radiative heat source profile that tends to warm the upper troposphere but may cool the surface (Liou 1986; Fu and Liou 1993; Fahey and Schumann 1999). Choi and Ho (2006) found that the longwave radiative forcing of cirrus clouds often exceeds the corresponding shortwave radiative forcing due to their low optical depth and cool ambient temperature that give rise to net surface warming of the Earth's surface.

Lidar (light detection and ranging) is a robust tool widely used for cirrus clouds studies, which include their identification and quantitative assessment (Saseen and Cambell 2001; Ramaswamy 2006; Nair et al. 2012; Das et al. 2009; Manoj Kumar et al. 2020; Lolli et al. 2020; Saha et al. 2020, 2021; Xie et al. 2017; Mbatha and Shikwambana 2022). The lidar can detect the cirrus cloud base and cloud top better than other techniques (Veerabuthiran 2004). It provides parameters such as normalized relative backscatter, extinction coefficient, backscatter and depolarization ratio, which help characterize the cirrus cloud (Das et al. 2009; Ramaswamy 2006; Nair et al. 2012; Manoj Kumar and Venkatramanan 2020; Manoj kumar et al. 2020). The majority of cirrus in the tropical region are subvisual and thin (Immler et al. 2007; Seifert et al. 2007) and cover up to 60%, which is mainly a result of anvils produced directly by deep convection in the inter-tropical convergence zone (ITCZ) and monsoonal circulations (Wylie et al. 1995; Chen and Liu 2005; Fortuin et al. 2007; Kox et al. 2014). Observational studies have indicated that during summer, the ITCZ continuously pumps moisture and aerosol from the lower troposphere into the upper, resulting in deep convection that often leads to cirrus clouds formation (Veerabuthiran 2004; Meenu et al. 2011). Das et al. (2011) reported the formation of tropical cirrus clouds coupled with the tropical easterly jet (TEJ) during the summer monsoon using CALIOP

and reanalysis data over the Asian Summer Monsoon region. The largest cirrus cloud occurrence is over the tropical Indian Ocean (SunilKumar and Parameswaran 2005; Seifert et al. 2007) as well as over the western Pacific (Heymsfield et al. 1998) and Southeast Asia (He et al. 2013; Wang et al. 2020), a significant fraction of which are optically and physically thin (Meenu et al. 2011). Cirrus clouds have a broad range of optical depths, positively and negatively impacting the radiation budget. Usually, thin cirrus clouds may produce positive radiative forcing at the top of the atmosphere, whereas there can be cooling due to thick cirrus clouds (Stephens and Webster 1981; Fu and Liou 1993; Fahey and Schumann 1999).

Cirrus cloud radiative transfer is one of the important components in the Earth heat budget equations. When these high cirrus clouds descend to lower altitudes, they can modify regional weather patterns (Prabhakara et al. 1993; Schumann et al. 2021). Cirrus descending with time is attributed to either gravitational settling of ice crystals within the cirrus or the downward movement of ice due to subsidence of upper tropospheric air mass (Heymsfield and Iaquinta 2000; Mitchell et al. 2008). The triggering mechanism for vertical movement could be due to atmospheric waves or general circulation. Nair et al. (2012) reported a descending pattern of cirrus in Trivandrum throughout the year, where they observed the maximum descending (1.5–2.5 km) in premonsoon and monsoon. The descent of cirrus can significantly modulate the moisture content and the radiation budget of the upper troposphere (Jakob 2001; Jensen et al. 2013). The ice particle content in cirrus undergoes sedimentation during its descent, resulting in the sublimation of these particles, increasing water vapour content at higher altitudes and significantly impacting radiative forcing (Jakob 2001; Jensen et al. 2013) subsequent to cloud formation.

The above studies have highlighted the role of cirrus clouds in the radiative balance of the Earth's atmospheric system, which usually depends on cirrus optical properties and vertical and horizontal coverage (Fu and Liou 1993; Zerefos et al. 2003; Seifert et al. 2007; Das et al. 2009). Due to limited knowledge of cirrus geometrical and optical properties, significant uncertainties remain with respect to the radiative and climate effects of cirrus clouds (Solomon et al. 2007; Stocker et al. 2013). Thus, observational studies can improve our present understanding of cirrus characteristics and their associated processes. In this context, we measured these clouds from July 2013 to June 2015 using a micro-pulse lidar over a coastal station (Goa) located on the west coast of India. This paper reports their characteristics, including occurrence, descending pattern and geometrical thickness during the study period. In addition, we will also discuss two cases of abnormal descending patterns during the summer monsoon and examine possible mechanisms responsible for such rapid descending of cirrus clouds. These results are further complemented by radiosonde and CALIPSO observations at the study site.

2 Site descriptions

The observational site is located at Goa (15.46 N, 73.8 E), a coastal station 40 m above the mean sea level on the west coast of India. The peculiar geography of Goa is such that the core of the southwest monsoon low-level jet (LLJ) passes through this region during the monsoon period (JJAS). The humid air stream undergoes topographic uplift when it meets the Western Ghats running parallel to the coastline. Topography-induced convection injects humid air deep into the troposphere, leading to cirrus clouds. Sufficient moisture is supplied from the monsoonal jets (LLJ and TEJ), and the convection associated with the inter-tropical convergence zone increases the formation of cirrus clouds over this region. The core of the TEJ (eastward) appears to pass above the LLJ (westward) at an altitude closer to the tropopause and generates a conducive atmosphere for the formation of cirrus (Das et al. 2011).

3 Data and methodology

3.1 Micro-pulse lidar system

The micro-pulse lidar (MPL) is an elastic backscatter lidar that operates at a wavelength of 532 nm with a high-pulse repetition frequency of approximately 2500 Hz, low-pulse energy of approximately 6–8 μJ and a pulse length of 9.3 ns. MPL consists of an optical transceiver unit, laser power supply and computer. The transceiver houses the laser transmitter and the photon counting detection system. A telescope with a diameter of 7–8 inches and a field of view 81.71 μrad is used for transmitting and receiving the laser pulses. The range resolved signal is collected and displayed in real time on the data acquisition computer. The transceiver is mounted on a swivel mechanism that is useful for elevation adjustment for vertical or off-zenith measurements. The data acquisition software SIGMA-MPL can also be used to play back data files recorded previously. The lidar operation is fully automated and designed for unattended data acquisition. The laser output energy from the telescope is designed to meet the ANSI Z136.1–2000 standard for eye safety. The receiver has depolarization measurement capability.

The temporal and vertical resolutions of the lidar were set to 30 s and 30 m, respectively. The parameters computed from the lidar are normalized relative backscatter (NRB) data, extinction coefficient, backscatter coefficient and depolarization ratio. NRB is calculated (following Eq. (1)) using the raw scattered photon counts, laser energy and instrument-specific correction terms and solving the system calibration coefficient through the lidar equation (Campbell et al. 2002).

$$NRB = \left[[Raw \times Deadtime - Afterpulse - Background] \times Range^2 \right] / (Overlap \times Laserenergy) \quad (1)$$

The backscattered signals are received in two channels known as CO-Polarization (NRB_{CO}) and CROSS-Polarization (NRB_{CROSS}). From the backscattered signal, the plane of polarization parallel and perpendicular to the laser is known as NRB_{CO} and NRB_{CROSS} , respectively.

The MPL installed at this site has additional features, such as an environmental protection chamber to safeguard it from external weather changes. This provides all-weather capability to generate uninterrupted data, making it a unique instrument compared to conventional lidar networks installed elsewhere. The MPL is widely used to detect cirrus (Spinhrne 1993; Campbell et al. 2002; Welton and Campbell 2002). Uninterrupted LIDAR data from July 2013 to June 2015 are considered for our present investigation.

3.2 Radiosonde observations

Uninterrupted ascents were carried out using all-digital Vaisala Radiosonde RS92-SGP, which measures pressure, temperature, relative humidity and wind profiles (instrument specifications and validation details are available online at <http://www.vaisala.com/en/meteorology/products/Pages/default.aspx>). The upper atmospheric profiles were collected every third day during monsoon months and weekly during non-monsoon months at 17:30 pm LT (LT = UTC + 05:30 h). Wind shear data were used to identify the meteorological condition for vertical oscillation of cirrus clouds during this study over Goa. The wind shear can be calculated by using the below described equation

$$wind\ shear = \frac{\sqrt{(V_1 - V_2)^2 + (U_1 - U_2)^2}}{\Delta Z} \quad (2)$$

where u , v and z is zonal wind component, meridional wind component and height, respectively.

3.3 ECMWF (European Centre for Medium-Range Weather Forecasts) reanalysis products

In addition to the above in situ observations, we also used the monthly climatology of temperature, relative humidity and zonal wind components from 2000 to 2014 from ERA-interim (<http://apps.ecmwf.int/datasets/data/interim-full-daily/levtype=sfc/>). ERA-Interim is the most widely used reanalysis dataset produced by the ECMWF. To identify seasonal variability over the study region, we downloaded data set from 15°N, 73°E to 16°N 74°E region with a spatial resolution of 0.125° × 0.125° latitude–longitude grid. ERA5 provides hourly estimates of several atmospheric, land and oceanic climate variables. It covers the entirety of the Earth

using 137 vertical levels ranging from the surface up to 0.01 hPa (~80 km). ERA5 is the most recent release of the data set provided by the ECMWF. One-hour vertical velocity data were downloaded for different pressure levels to pick vertical velocities collocated with descending cirrus during the descending event.

3.4 Identification of cirrus clouds

Cirrus clouds are detected from the linear depolarization ratio, which mainly calculates the scattering nature and shape of aerosols and clouds. The ratio of the plane of polarization perpendicular to the laser to the plane of polarization parallel to the laser is called the linear depolarization ratio (LDR) (Ramaswamy 2006; Flynn et al. 2007; Eq. (3)).

$$LDR = \frac{NRB_{CROSS}/NRB_{CO}}{[NRB_{CROSS}/NRB_{CO} + 1]} \quad (3)$$

LDR is a measure of sphericity of the particles wherein a higher depolarization ratio refers to higher nonsphericity and vice versa (Muller et al. 2006; Rajeev et al. 2010; Saha et al. 2020; 2021). Lidar measurements are widely used in the Indian region to investigate the characteristics of aerosols and clouds (Satheesh et al. 2006; Rajeev et al. 2010; Saha et al. 2021). Atmospheric hydrometeors (rain or cloud) scatter more photons than carbonaceous, sea salt and dust aerosols (Ramaswamy 2006). In the case of clouds, the scattering property differs from water clouds to icy clouds (Uchino et al. 1988; Nair et al. 2012). Therefore, clouds are identified using their scattering properties and their height of occurrence (Nair et al. 2012). Typically, most cirrus clouds are located near the tropopause (~18 km) but are observed anywhere between 8 and 18 km (Pandit et al. 2015; SunilKumar et al. 2010). However, according to Veerabuthiran (2004), tropical cirrus can be seen as low as 6 km. Cirrus clouds are often defined as nonspherical high icy clouds with LDRs higher than aerosols (Krämer et al. 2009; Jeffery and Austin 1997). Supplementary Figure S1(a and b) represent typical examples of cirrus occurrences observed through the MPL retrieval and compared with same day image from the CALIPSO (Figure S1 c). In this study, we used LDR to detect typical features of cirrus clouds such as their occurrence and descent. The cirrus cloud top and bottom were identified as a sudden increase and decrease in LDR values with respect to the height (a typical example is provided in Supplementary Figure S2). In this study, the cirrus identification was made based on LDR only, as reported by several workers from coastal India (Nair et al. 2012; Manoj Kumar et al. 2020). In addition, we have also compared cirrus identification using LDR and NRB to assess the robustness

of methodology (Figure S2), which clearly shows cloud base and top are at a similar height in both NRB and LDR plots. Using lidar measurements, Chen et al. (2002) examine cirrus clouds in Chung-Li, Taiwan. They found that cirrus clouds LDR from 0.2 to 0.5 between 11 and 15 km height; above 15 km, LDR is ~0.3. SunilKumar and Parameswaran (2005) have studied cirrus optical properties over the tropical region using LDR, where they found that LDR increases with decreasing temperature. Ramaswamy (2006) defined cirrus clouds with LDR greater than 0.4 in Alaska, whereas Nair et al. (2012) defined LDR for cirrus clouds in the troposphere greater than 0.05 in Trivandrum, India. Considering previous studies and from daily visual observations at the study site, LDR value for cirrus is taken as > 0.09. The majority of time MPL was operated with 30-m vertical resolution and 30 s of time resolution and those having a residence time of more than 5 min were considered in this study. Most cirrus clouds and their descending pattern were observed during the afternoon time. The lidar data exhibit more clarity on cirrus structures which are observed during late evening than those observed during daytime owing to poor signal-to-noise ratio and contamination by background photon counts (Dupont et al. 2011). An optically thick high reflective cloud is observed during monsoon months and calculated by taking the difference between top and bottom height of the cirrus cloud.

4 Results and discussion

4.1 General meteorological conditions over Goa

Goa is situated on the central west coast of India in the latitudinal belt of 13° to 17° N. Figure 1 a, b and c show the climatological mean of zonal wind, relative humidity and temperature respectively. It is interesting to note that the wind and humidity patterns show clear seasonal variations. The subtropical westerly jet streams in the upper troposphere (approximately 300 mb) are visible in all months except the southwest monsoon season (SWM; June–September). During this period, the subtropical jet is replaced by a tropical easterly jet in the upper troposphere, and a monsoon low-level jet exists at approximately 850 mb. These two jets are important synoptic components of the Indian summer monsoon (Joseph and Raman 1966; Koteswaram 1958). The LLJ appears to carry moisture from the Arabian Sea through wind-sea surface temperature-evaporation feedback, while the TEJ acquires moisture from the LLJ uplift at the Tibetan Plateau, and its course over the Bay of Bengal makes conducive conditions for cirrus formation (Pfister et al. 2001; Fu et al. 2007; Chen and Liu 2005; Corti et al. 2006). Relative humidity parameters show large values even up

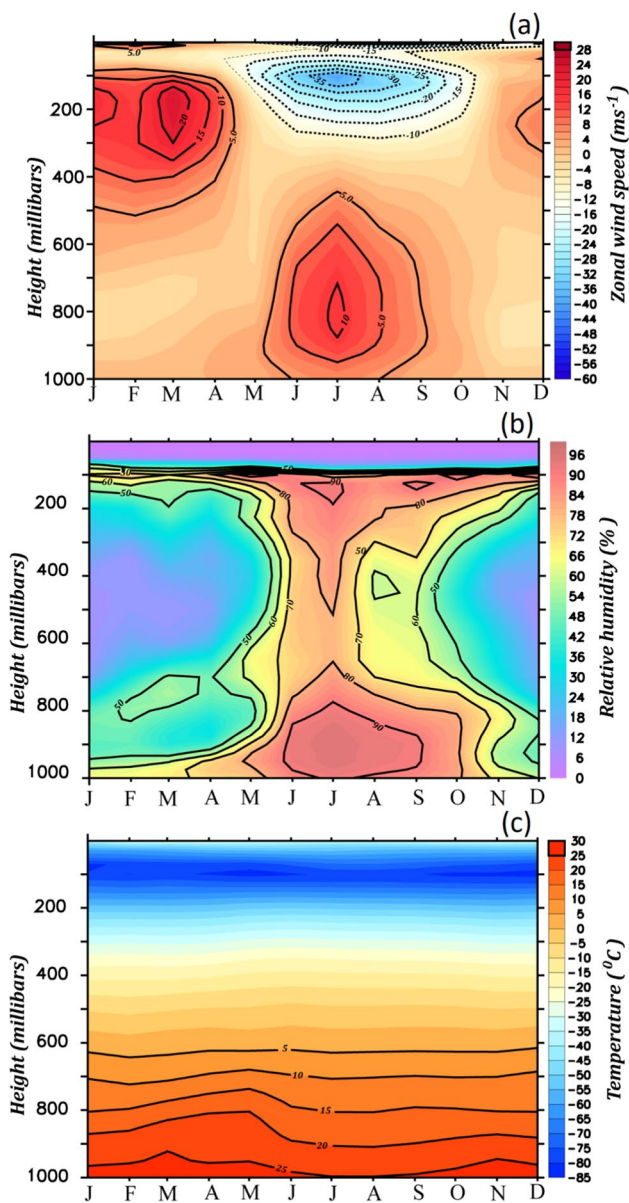


Fig. 1 Climatology of the monthly mean **a** zonal wind, **b** humidity and **c** temperature over the study site (Goa; 15–16°N and 74–75°E)

to the troposphere in the SWM season, indicating the moisture abundance in the whole troposphere (Fig. 1b). From Fig. 1c, it is evident that the premonsoon months exhibit relatively higher temperatures than any other season. Since these parameters have an influential role in cirrus formation and its associated features, this analysis will be useful in characterizing the monthly and seasonal distribution and properties of cirrus over the study region. Detailed analyses and discussions on the characteristics of cirrus and its descending nature over the coastal station will be discussed in the following sections.

4.2 Characteristics of cirrus occurrence

From the lidar observations made over Goa during the study period from July 2013–June 2015, it is clear that the cirrus occurs in all four seasons. Of 695 total observations taken during the study period, cirrus occurrence was noticed on 383 occasions. Figure 2 describes the properties of cirrus occurrence. Except for January 2014 and June 2015, the LIDAR was operated continuously (more than 25 days) throughout the year.

Figure 2 a shows a higher number of occurrences during June–December, with the maximum event in September and the lowest occurrence in February. A clear seasonal variation is observed in cirrus occurrences, as seen in Fig. 2b. The maximum is seen during the southwest monsoon (44%), followed by the postmonsoon (33%). Winter months show the lowest occurrence frequency (6%). A similar pattern has been reported from Trivandrum (Nair et al. 2012) on the west coast of India and in Gadanki on the east coast of south India (Manoj Kumar et al. 2020), where the maximum occurrence is observed in (Trivandrum = ~69%; Gadanki = ~90%) the southwest monsoon and a minimum occur during winter (Trivandrum = ~36%; Gadanki = ~55%).

The monthly mean and standard deviation of the cirrus cloud geometrical thickness are shown in Fig. 2c. A higher geometrical thickness is observed in the period August–November with the maximum (1.9 ± 0.9) in September (1.9 ± 0.9) and the minimum in February (0.3 ± 0.25). Most tropical cirrus cloud thicknesses can be less than 2 km, and some can be up to 3 km (Veerabuthiran 2004). Analyses of both the cloud base (CB) and cloud top (CT), which are provided in Table 1, reveal that both show minimum and maximum values during the southwest monsoon and winter seasons, respectively. The persistence of cirrus clouds at lower altitudes (~4.5 km) during the southwest monsoon might have been influenced by ambient conditions such as moisture availability, as described in the previous section.

4.3 Descending nature of cirrus clouds

An interesting factor associated with cirrus occurrence is its descending nature. We have calculated the descending characteristics of cirrus clouds such as displacement and time by using the LDR method. This involves the analysis of LDR height profiles at each time step. Cirrus cloud base and top is calculated based on the sudden increase and decrease in the LDR height profile. Descending height is calculated as the difference between the final and initial heights of the cirrus cloud base. The time of descent is calculated as the time taken for the descent. A total of 163 cases of descending cirrus were observed during this study period. The descent of cirrus clouds often occurs due to

Fig. 2 **a** Monthly average cirrus occurrences (%) shown as bar diagram and number of days when lidar was operational (solid line with closed circle). **b** Pie chart showing frequency of occurrence of cirrus in different seasons. **c** Monthly average cloud geometrical thickness during 2013–2015

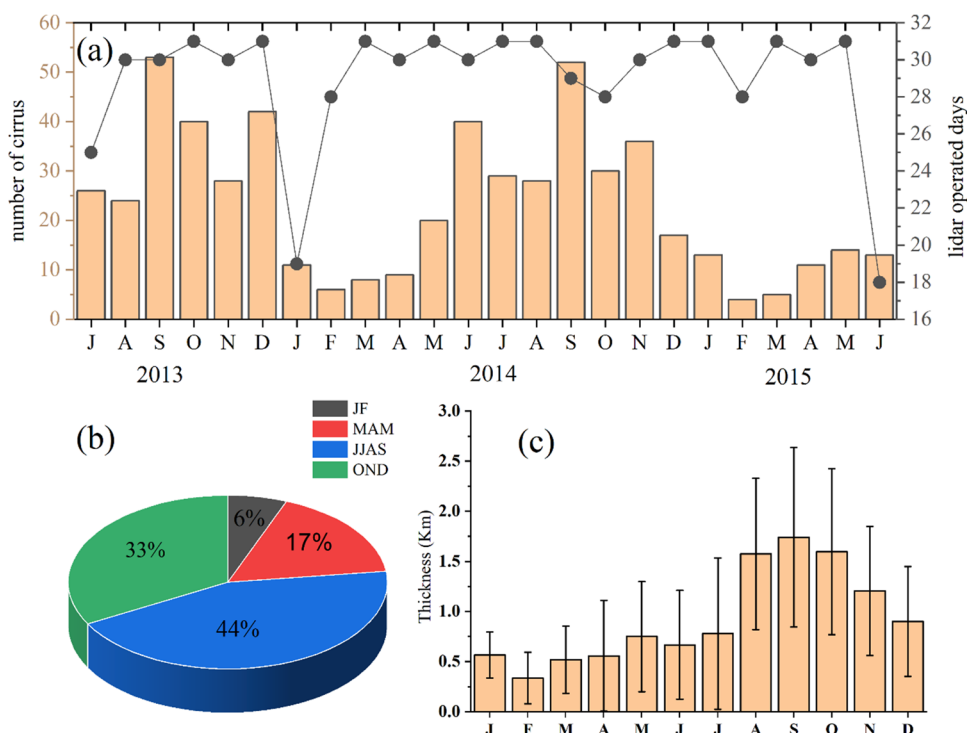


Table 1 Monthly mean and SD of CB and CT of cirrus clouds (in km)

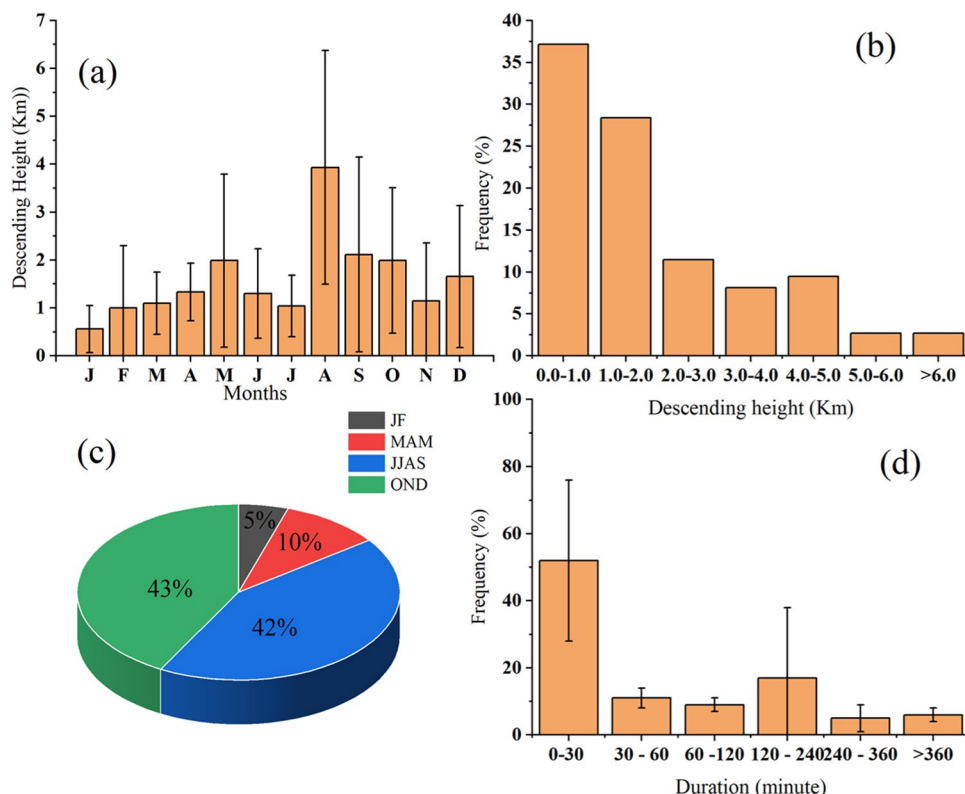
Month	Cloud base (CB)		Cloud top (CT)	
	Mean	SD	Mean	SD
January	13.13	1.01	14.05	1.07
February	13.29	2.23	13.87	1.96
March	11.32	2.53	12.26	2.11
April	12.43	2.96	13.43	2.91
May	12.96	2.17	14.20	1.88
June	10.66	2.59	12.00	2.87
July	9.17	2.45	10.46	2.78
August	10.73	1.33	12.86	1.54
September	10.63	2.28	13.08	2.01
October	11.43	2.12	13.22	1.96
November	12.35	1.34	13.80	1.07
December	13.00	1.96	14.28	1.44

the subsidence of upper tropospheric air masses associated with sedimentation, atmospheric waves, atmospheric disturbance, general circulation or several other coupled processes (Heymfield and Iaquinta 2000; Mitchell et al. 2008; Nair et al. 2012; Immler et al. 2007; Das et al. 2013). Nair et al. and Manoj Kumar et al. (2012) observed the descending nature of cirrus clouds over the Indian region, as discussed earlier. A similar result was reported by Sharma et al. (2015) in Ahmedabad. They observed a descending or ascending (downdraft and updraft) nature of low and middle clouds

during the southwest monsoon and postmonsoon periods. Figure 3 represents the duration and frequency of descending height over different periods in Goa. Figure 3 b suggests that the majority of descending height occurs below 2 km, and in very few cases, it descends above 6 km height.

This result resembles those reported by Manoj Kumar et al. (2020) over Gadanki, India, where most of the cirrus descent height was observed below 1 km. The monthly distribution of cirrus descending (Fig. 3a) shows that descending is frequent in latter half of the year, particularly from August to December. Maximum descending is observed in August (4 ± 2.4 km) and minimum in January (0.5 ± 0.5 km). The seasonal maximum frequency of descending is observed in the southwest monsoon season (43%), which is followed by the postmonsoon (42%) and the lowest frequency is observed in winter (5%) (Fig. 3c). Nair et al. (2012) observed a maximum of cirrus descending in the premonsoon months and a minimum in winter at Trivandrum. Our study region and Trivandrum are in the same longitudinal belts but different latitudinal belts. The frequency distribution of duration of cirrus descent explains (Fig. 3d) that almost half of the cirrus descent occurred within half an hour. Another striking feature observed during this study is that more than 30% of the cases had durations above 2 h. This is important because descent cirrus significantly affects the radiative feedback processes in the atmosphere (Nair et al. 2012). The longer duration will have a significant influence on the radiation feedback process. The influence of cirrus descent on the radiative feedback is covered in detail in the latter part of the discussion.

Fig. 3 **a** Monthly average descending of cirrus clouds during 2013–2015; **b** frequency distribution of descending cirrus clouds; **c** relative percentage contribution of descending cirrus clouds in different seasons and **d** frequency of duration of cirrus descent



To further investigate the descending nature, probability distribution function (PDF) analysis is carried out and presented in Fig. 4. Figure 4 a depicts the PDF of vertical displacement of the cloud top versus the cloud base. This indicates that a one-to-one relationship exists between the vertical displacements of cloud bottom and top, resembling those reported by Nair et al. (2012) and Manoj kumar et al. (2020). The mean displacements of the cloud top and bases are 1.97 ± 1.92 and 2.16 ± 1.99 km, respectively. The downward displacement occurred mostly within the 0–3-km range. This result corroborates that the descent most often occurred below 3 km (Fig. 3). Figure 4 b and c display the

PDF of cirrus cloud altitude before and after the descent for the cloud base and cloud top respectively.

The term “before” is used when the cirrus cloud is at particular height which is just about to start the descent process and “after” is used when the cirrus cloud reaches at a particular height level after descent. Figure 4 b represents the cloud base information and indicates that the maximum occurrence probability for the cloud base is in the range 10–15 km and 8–14 km before and after the descent respectively, whereas, Fig. 4c contains the information on the cloud top before and after the descent and their respective values are in the range 12–16 km. These

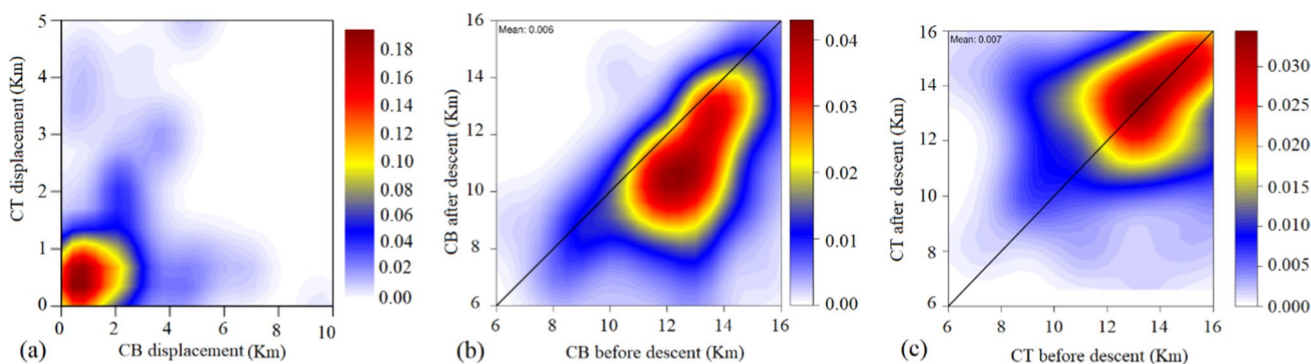


Fig. 4 **a** Probability distribution functions of the cloud base and top vertical displacement for the cirrus descent; **b** cloud base before descent versus after descent; **c** cloud top before descent versus after descent

figures show that the descending cirrus shows almost uniform displacement at all altitudes, although there is considerable spread in its distribution. Figure 5 a and b clearly show that the cirrus descending time is usually within 1 h and that the displacement and geometrical thickness are less than 1 km. We have calculated the descending speed of each case of cirrus with a noticeable descending height. The speed of cirrus is calculated as the difference between the descending height of the cloud base before and after descent divided by the duration of that descending event. To assess the descending speed behaviour with the duration of descent, we plotted PDF shown in Fig. 5c and d. Here, we considered only those cases where the descent is greater than 1 km. The maximum probability is confined to the longer duration time with slower descending speed. The correlation coefficient between the descending speed and duration for both cases (cloud base and cloud top) are -0.25 and -0.30 , respectively. This relation is significant at 1% confidence level. Thus, we conclude that descent speed is inversely proportional to the duration of descent. Nair et al. (2012) found a similar inverse relationship in Trivandrum, India. Out of 124 cases, 90% had a duration greater than 2 h. The median descending speeds for both the cloud base and top were found as 0.07 and 0.06 m/s, respectively.

4.4 Rapid descent of cirrus clouds: a case study

During the observational period, there were 25 cases of significant cirrus descending (displacement greater than 3.5 km). Of these, two extreme cases were observed in September 2013 and August 2014 during the monsoon period

with a displacement of more than 7 km. These extreme cases will be discussed in detail in the subsequent paragraphs. The lidar depolarization ratio patterns associated with descending cirrus clouds during 2013 and 2014 are illustrated in Fig. 6b and d. The cirrus appears to be gradually descending (7.8 km in approximately 11.6 h) in 2013 from approximately 15 km to about 7 km in a humid atmosphere where the relative humidity (RH) varied from 50 to 70% (Fig. 4a) and hence tends to retain its geometrical thickness and nonsphericity to certain extent before dissipating. In contrast, abruptly descending thin cirrus is observed in a relatively dry (RH \sim 20%) ambient atmosphere during 2014 (Fig. 6c and d). The descending cirrus is noticed here from approximately 14 to 4.4 km (9.6 km in 6.5 h). The low depolarization and decreasing nonsphericity are associated with melting and thinning of cirrus in a warming atmosphere (rapid increasing pressure) which possibly culminate in the form of precipitation as it crosses the threshold temperature shown by the low depolarization ratios (less than 0.1) (Fig. 6d). Typically, cirrus clouds form when moisture is supported by an ambient temperature colder than -20 °C (Veerabuthiran 2004). The shape and size of ice crystals in the cirrus vary due to gravitational pulling and turbulence. Humidity profiles indicate deep penetration of humid air crossing the -20 °C isotherm enabling thick cirrus formation in 2013 (Fig. S3 b and c) compared to the intermittent and less organized convection associated with a relatively weak monsoon of 2014 (Fig. S3 e and f). Another factor affecting the cirrus distribution and its descent is the vertical wind shear (detailed calculation is provided in Sect. 3.2). During the southwest monsoon, effect of the TEJ is observed up to 10-km altitude with a speed of > 10 m/s (Fig. S3 a and d). The LLJ is predominantly

Fig. 5 **a** Probability distribution functions of cirrus descent duration versus geometrical thickness; **b** descending height; **c** descending speed of cloud base and **d** descending speed of cloud top

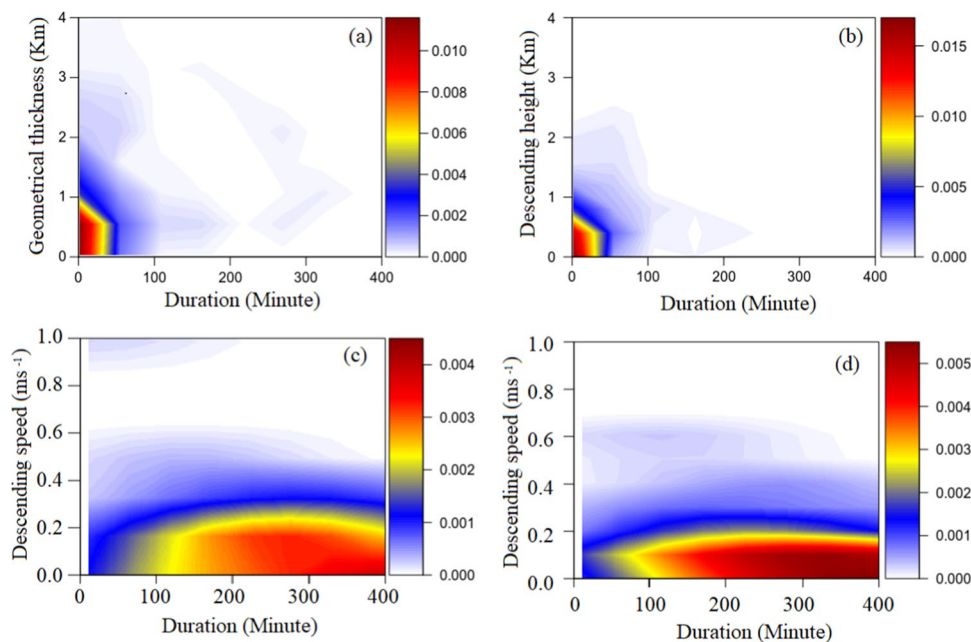
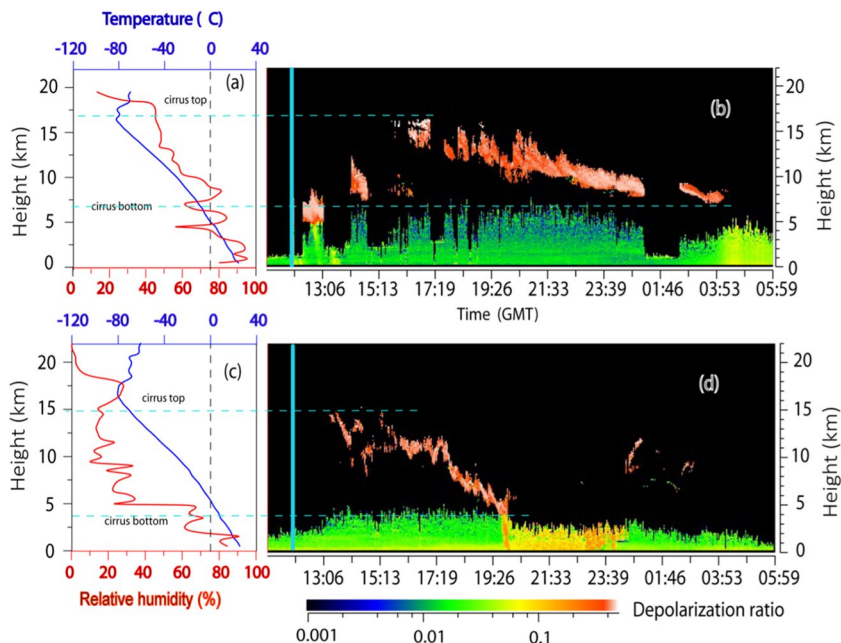


Fig. 6 Vertical profile of temperature and relative humidity obtained from the RS92 Vaisala radiosonde during **a** 14–15 September 2013 and **c** 22–23 August 2014. Cirrus oscillation pattern observed from MPL backscatter time series data (time in GMT) during **a** 14–15 September 2013 and **c** 22–23 August 2014 (time in GMT for LIDAR data and 5:30 IST time for radiosonde observation) partially coinciding with the cirrus descending stretch

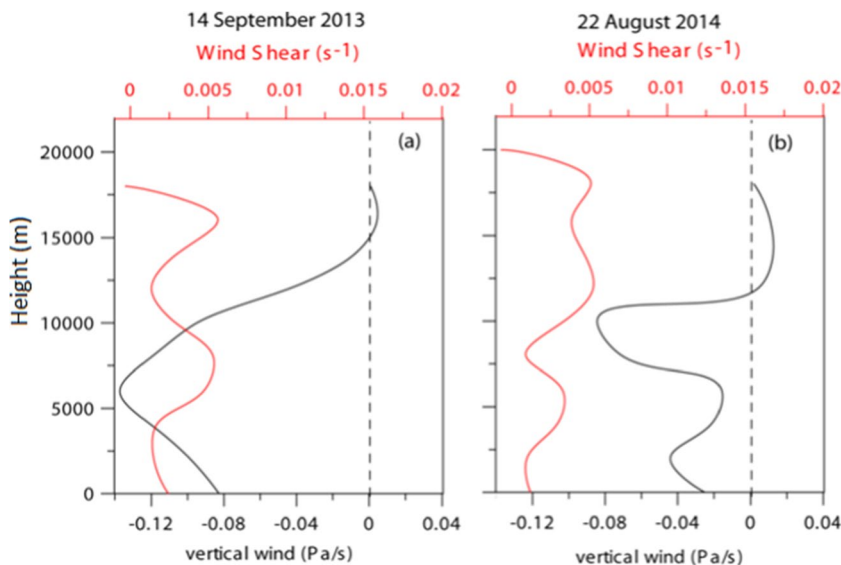


westerly in direction, whereas the TEJ is easterly. Thus, these fast-flowing air currents in opposite direction can create strong wind shear in the troposphere (Fig. 1 and Fig. S2). Both jets (LLJ and TEJ) are well developed in 2013 compared to 2014. However, the vertical stretch of the core of TEJ appears to be larger in 2014 than in 2013. Moreover, the well-developed LLJ and TEJ spread right across the southwest monsoon months in 2013 and thus have greater impact on the geometrical thickness of the cirrus, while the larger vertical stretch of TEJ in 2014 contributes to the dynamics associated with the wind shear compared to 2013.

To obtain more clarity on these descending processes, we investigated the inter-relationship of wind shear and

vertical air movement during the two extreme cases of cirrus descending. The vertical velocity profiles were plotted against the radiosonde derived wind shear during the period of cirrus descending (Fig. 7). This comparison has inherent limitations as vertical wind velocity is a gridded reanalysis product with uncertainties. Despite this, the comparison is possible, as the magnitude of vertical velocity fluctuates with the perturbations in wind shear irrespective of the polarity. However, the influence of shear in changing polarity is unclear from Fig. 7. The two high wind shear zones in Fig. 7a (17 km and 7 km) and in Fig. 7b (15 km and 11 km) roughly coincide with the enhanced vertical wind with some phase shift. Therefore, the vertical velocity

Fig. 7 Vertical variation in wind shear and vertical velocity plotted over Goa for **a** 14–15 September 2013 and **b** 22–23 August 2014



with time appears to vary with the fluctuations in wind shear triggered by the resultant currents at various levels in the vertical plane.

We also investigated the influence of vertical velocity on the descending structure of cirrus clouds in the troposphere. The positive vertical velocity in the pressure coordinate explains downward motion and a negative value denotes an upward motion. The vertical velocity data with hourly resolution from radiosonde are not possible; thus, we used the vertical velocity from Era-5 reanalysis data (which shows good correlation with the radiosonde data; Figure S4 and S5). The vertical velocity profile (ERA-5) during the cirrus descending period is reproduced in Fig. 8a and b. The outline of the cirrus cloud (shaded in grey colour) obtained in September 2013 and August 2014 is superimposed on the vertical velocity field to gauge impact of atmospheric forcing to yield the observed descending structure. The variation of the vertical velocity across the cirrus descending is plotted

every hour of the descending period and reproduces the variability as a line graph against unit of time in Fig. 8c and d.

The cirrus structure in both year acts according to the direction of vertical velocity, where negative velocity tends to lift it in the former half of the cirrus and positive velocity tends to push it down at the latter half of the cirrus (Fig. 8c and d). Therefore, descending pattern of the cirrus in both cases can be explained by this descending, which appears to be gradual during 2013 (Fig. 8a) in the time window of 1700 h (22:30 h IST) to 0400 h (09:30 h IST) the next day. Here, the vertical wind pattern is such that the cirrus roughly lies parallel to the velocity contour while crossing over to a positive wind regime, making the transition gradual. In contrast, during August 2014, the weak negative vertical velocity does not provide the required momentum until it enters the opposite polarity regime where cirrus passes right across the velocity contour to reach close to the core

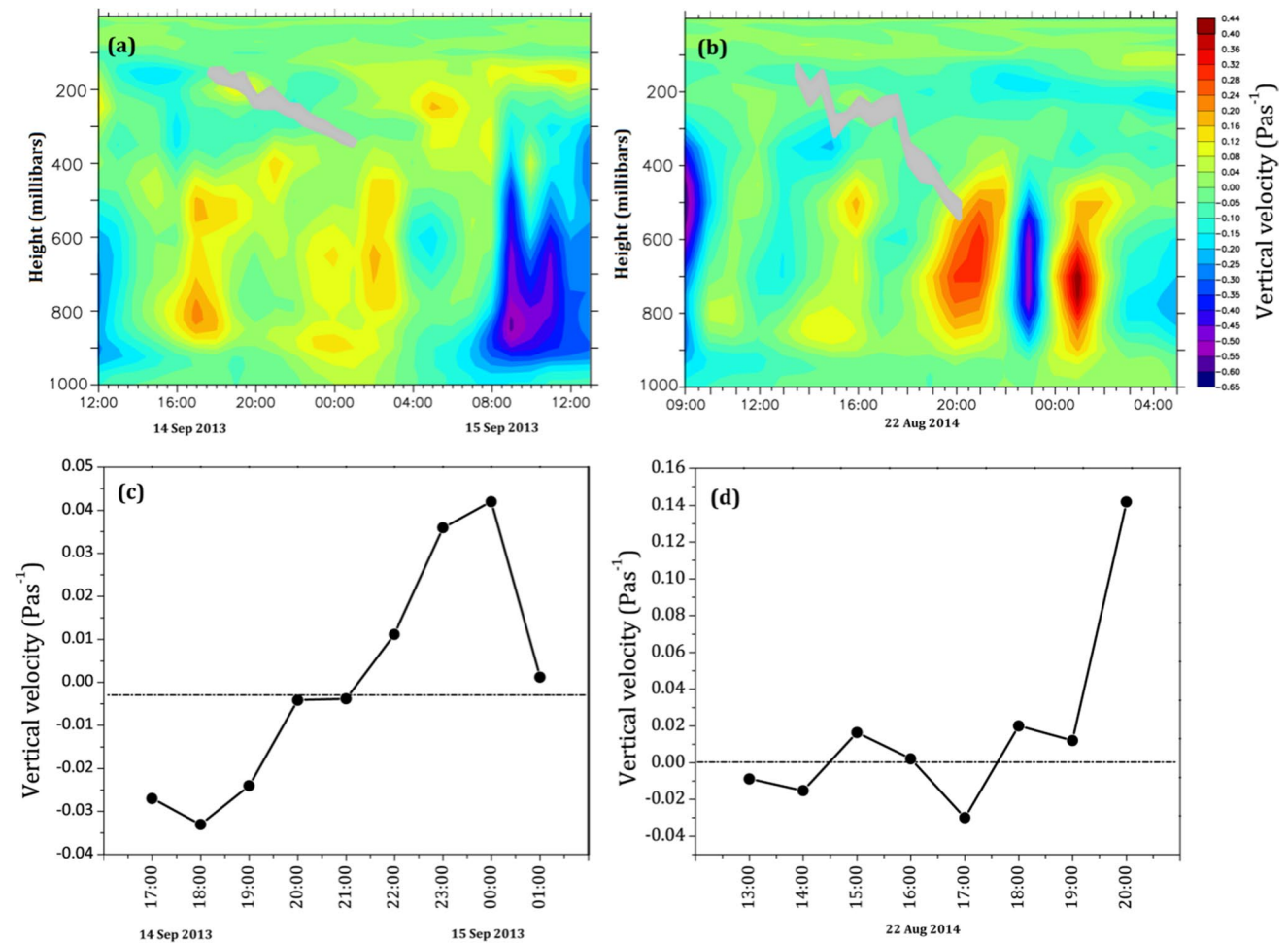


Fig. 8 Vertical velocity (shaded) profiles in the troposphere are plotted with time during the period of cirrus descent in **a** September 2013 and **b** August 2014. The rough outline of the cirrus (shaded in grey) is superimposed over the velocity field. Altitude is given on the

Y-axis in terms of pressure (mb) and height (km). Vertical velocity is plotted every 1 h across the cirrus axis during the period of descent in **a** 2013 and **d** 2014. Negative velocity refers to upward thrust, and positive velocity refers to downward thrust

in a short possible time (Fig. 8b) enabling, a sharp descent (in less than an hour).

The pressure difference increases temperature and dissipates cirrus, causing ice to melt in the form of precipitation, as shown by the lidar depolarization values (a decrease in nonsphericity) close to the surface (Fig. 6d).

The cloud cover would lead to more sunlight reflected into space. In contrast, the trapping of atmospheric thermal emission by cirrus clouds enhances the radiative energy (heat) in the atmosphere and the surface (Liou 1986; 2002; Schumann 2002). Various studies have shown that cirrus clouds cause warming effects in the tropics and cooling effects in the mid-latitudes (Sivakumar et al. 2003; Nicolas and Bromwich 2011). One of the major implications of the cirrus descent is the reduction of longwave cloud radiative forcing at the top of the atmosphere by 1 to 12.9 Wm⁻² (Nair et al. 2012). Here we attempted to address another impact of cirrus descending on the regional weather in terms of surface warming during various phases of cirrus descending. To achieve this, we have chosen a few cases of cirrus descending where the vertical displacement is higher than 5 km.

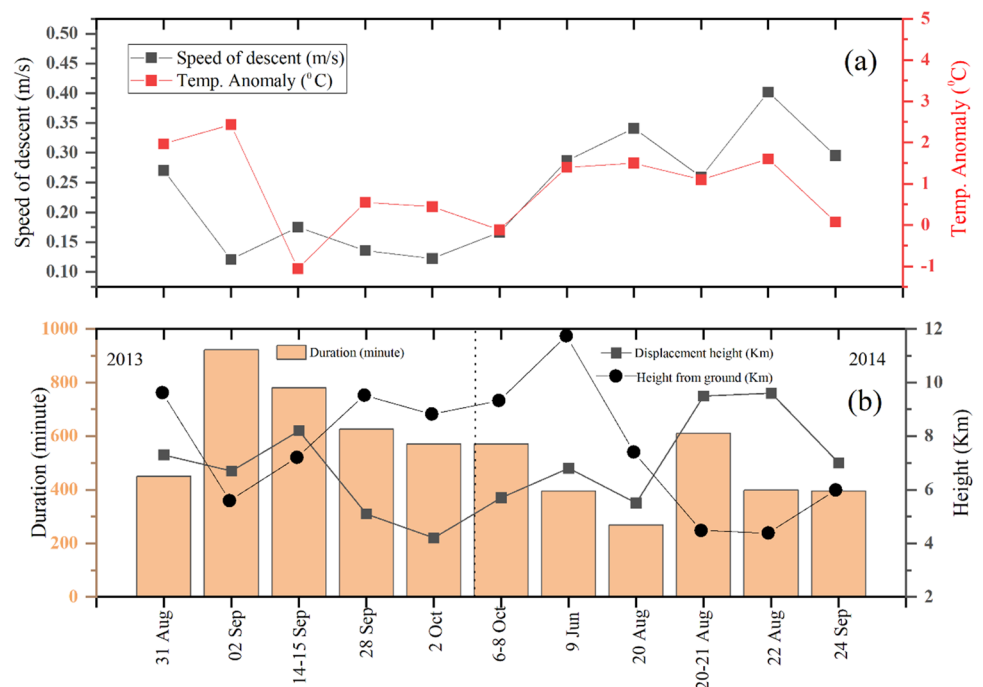
The cirrus descending cases have been categorized based on duration, vertical displacement, height from the ground and descending rate derived from lidar data and compared with surface temperature anomaly derived from surface automatic weather station (AWS) data during 2013 and 2014 (Fig. 9). The daily temperature anomalies were calculated from the 2009 to 2015 period data. There are few days where group of cirrus are observed continuously for two to three days (6–8 October 2013, 21–22 August 2014); in that case, we have averaged it

for two days of anomaly. Out of eleven cases, nine indicated an appreciable temperature rise during the cirrus descending indicating a possibility of 82% (Fig. 9a). The rate of descending appears to be higher in 2014 with values ranging between 0.14 and 0.4 m/s while during 2013, relatively lower descent rates were observed (Fig. 9a). The strong convection and high rainfall during 2013 probably influenced the descending pattern of cirrus in contrast to those observed during 2014. Strong convection often inhibits vertical displacement, as seen in 2013. When the duration of cirrus descending correlates more with surface warming during 2013, the vertical displacement of cirrus is likely to associate with the positive temperature anomaly in 2014 (Fig. 9). In short, the duration of cirrus descent is one of the key factors for the rise in temperature during the intense monsoon season, while vertical displacement is key to the temperature rise in weak monsoon months. These conclusions are based on the 2-year data set and relatively longer time series observational (collocated radiosonde and lidar) data can provide more robust information.

5 Summary

This study reports cirrus clouds seasonal distribution from the lidar backscatter profiles from July 2013 to June 2015. These observations are corroborated with continuous radiosonde profiles of humidity, temperature and wind to assess the formation and dynamics of cirrus clouds from a coastal station on the west coast of India. Major outcomes are:

Fig. 9 a Descending rate (black rectangle dot and line) and temperature anomaly (red rectangle and line); b duration (colour bar), displacement height (black closed rectangle and solid line) and descending height from the ground (black closed circle and solid line) for each cases of cirrus cloud descending pattern over the study region



1. Using MPL data, we monitored cirrus cloud characteristics and descending nature over a coastal station in the eastern Arabian Sea.
2. The frequency of cirrus occurrence is maximum in the southwest monsoon and lowest in the winter season. Optically thicker clouds were observed in the monsoon whereas, in the postmonsoon, cirrus occurred often.
3. Out of several occurrences of oscillating cirrus clouds, very few exhibited tendencies of descending patterns with displacements greater than 4 km during monsoon months.
4. Two extreme cases have been chosen from this group with more than 7 km displacement during September 2013 and August 2014 to investigate the dynamics associated with this rare oscillation.
5. The speed of descent in 2014 (0.4 m/s) was twice the speed (0.2 m/s) observed in 2013. This is possibly, the first observation of extreme cirrus descent reported from the Indian coastal region. Comparatively thick cirrus was observed in 2013 compared to 2014. The zonal wind pattern of 2013 differs much from that of 2014, as both LLJ and TEJ were well organized and evenly distributed month wise during September 2013. The core of the TEJ was stronger during the peak monsoon month of August 2014 and its vertical extent often generates relatively strong wind shear compared to September 2013. This anomalous wind shear triggers sharp vertical oscillation in the mid-troposphere. The gradual tilt observed in September 2013 was because the cirrus axis aligns more or less parallel to the velocity contour while in August 2014; the cirrus axis stretches across the velocity contours to provide a rapid downward tilt at the latter half of the cirrus.

Supplementary Information The online version contains supplementary material available at <https://doi.org/10.1007/s00704-023-04518-w>.

Acknowledgements The work is carried out under the institutional program “Geosinks” funded by Council of Scientific and Industrial Research, Government of India. Authors are grateful to Mr. Ajilesh P, DAS, CUSAT, for the essential technical support provided for this work. We appreciate the Editor and anonymous reviewer suggestions for improving the manuscript. This is NIO contribution number 7087.

Author contribution A. K., V. R. and P. M. M. conceived the idea and designed the research. A. K., P. M. M. and M. A. A. conceptualized and planned the measurement of clouds using LIDAR. A. K. and M. A. A. have done processing of data and analysed all parameter with the help from V. R., P. M. M., R. D. R. and S. K. D. M. A. A. performed the data interpretation with help from R. D. R., S. K. T. and A. K. M. A. A. wrote the first draft of the manuscript under the mentorship of AK with critical edits and inputs from R. D. R. and comments from S. K. D. All the co-authors discussed the results and commented on the manuscript.

Funding This work is carried out under the institutional program “Geosinks” funded by CSIR-National Institute of Oceanography, India as well as DST INSPIRE Faculty (IF-13-EAS-13). M. A. A. thank CSIR, Govt. of India, for providing partial financial support under the Senior Research fellowship.

Data availability The authors confirm that the data supporting the findings of this study are available within the article and/or its supplementary materials.

Code availability Not applicable.

Declarations

Ethics approval Not applicable.

Consent to participate Not applicable.

Consent for publication Not applicable.

Conflict of interest The authors declare no competing interests.

References

- Ali S, Mehta SK, Ananthavel A, Reddy TVR (2022) Temporal and vertical distributions of the occurrence of cirrus clouds over a coastal station in the Indian monsoon region. *Atmos Chem Phys* 22(12):8321–8342
- Ananthavel A, Mehta SK, Ali S, Reddy TVR, Annamalai V, Rao DN (2021) Micro pulse lidar measurements in coincidence with CALIPSO overpasses: comparison of tropospheric aerosols over Kattankulathur (12.82 oN, 80.04 oE). *Atmos Pollut Res* 12:101082
- Baran AJ (2009) A review of the light scattering properties of cirrus. *J Quant Spectrosc Radiat Transf* 110:1239–1260
- Baran AJ (2012) From the single-scattering properties of ice crystals to climate prediction: a way forward. *Atmos Res* 112:45–69
- Burkhardt U, Kärcher B (2011) Global radiative forcing from contrail cirrus. *Nat Clim Chang* 1:54–58. <https://doi.org/10.1038/nclimate1068>
- Campbell JR, Hlavka DL, Welton EJ, Flynn CJ, Turner DD, Spinhirne JD, Stanley S, Hwang IH (2002) Full-time, eye-safe cloud and aerosol lidar observation at atmospheric radiation measurement program sites: instruments and data processing. *J Atmos Ocean Technol* 19:431–442. [https://doi.org/10.1175/1520-0426\(2002\)019%3c0431:FTESCA%3e2.0.CO;2](https://doi.org/10.1175/1520-0426(2002)019%3c0431:FTESCA%3e2.0.CO;2)
- Campbell JR, Dolinar EK, Lolli S, Fochesatto GJ, Gu Y, Lewis JR, Marquis JW, McHardy TM, Ryglicki DR, Welton EJ (2021) Cirrus cloud top-of-the-atmosphere net daytime forcing in the Alaskan subarctic from ground-based MPLNET monitoring. *J Appl Meteorol Climatol* 60:51–63
- Campra P, Garcia M, Canton Y, Palacios-Orueta A (2008) Surface temperature cooling trends and negative radiative forcing due to land use change toward greenhouse farming in south eastern Spain. *J Geophys Res Atmos* 113(D18)
- Chen B, Liu X (2005) Seasonal migration of cirrus clouds over the Asian Monsoon regions and the Tibetan Plateau measured from MODIS/Terra. *Geophys Res Lett* 32(1)
- Chen T, Zhang Y, Rossow WB (2000) Sensitivity of atmospheric radiative heating rate profiles to variations of cloud layer overlap. *J Clim* 13:2941–2959. [https://doi.org/10.1175/1520-0442\(2000\)013%3c2941:SOARHR%3e2.0.CO;2](https://doi.org/10.1175/1520-0442(2000)013%3c2941:SOARHR%3e2.0.CO;2)
- Chen WN, Chiang CW, Nee JB (2002) Lidar ratio and depolarization ratio for cirrus clouds. *Appl Opt* 41(30):6470–6476
- Choi YS, Ho CI (2006) Radiative effect of cirrus with different optical properties over the tropics in MODIS and CERES observations. *Geophys Res Lett* 33:1–6. <https://doi.org/10.1029/2006GL027403>
- Clouds and Climate (2020) *Clouds Clim*. <https://doi.org/10.1017/9781107447738>

- Corti T, Luo BP, Fu Q, Vömel H, Peter T (2006) The impact of cirrus clouds on tropical troposphere-to-stratosphere transport. *Atmos Chem Phys* 6(9):2539–2547
- Dai G, Wu S, Song X, Zhai X (2018) Statistics of optical and geometrical properties of cirrus cloud over tibetan plateau measured by lidar and radiosonde. *EPJ Web of Conf* 176:05040 (**EDP Sciences**)
- Das SK, Chiang CW, Nee JB (2009) Characteristics of cirrus clouds and its radiative properties based on lidar observation over Chung-Li, Taiwan. *Atmos Res* 93:723–735. <https://doi.org/10.1016/j.atmosres.2009.02.008>
- Das SK, Chiang C-W, Nee J-B (2011) Influence of tropical easterly jet on upper tropical cirrus: an observational study from CALIPSO, Aura-MLS, and NCEP/NCAR data. *J Geophys Res* 116:D12204. <https://doi.org/10.1029/2011JD015923>
- Das SK, Das SS, Chiang C-W, Nee J-B (2013) Descending cirrus associated with planetary scale disturbance: an observational study from lidar, radiosonde and reanalysis data. *J Atmos Solar-Terrestrial Phys* 104:137–147
- Dupont JC, Haeffelin M, Morille Y, Comstock JM, Flynn C, Long CN, Sivaraman C, Newson RK (2011) Cloud properties derived from two lidars over the ARM SGP site. *Geophys Res Lett* 38(8)
- Fahey DW, Schumann U (1999) Aviation-produced aerosols and cloudiness. In: Penner JE et al (eds) *Aviation and the Global Atmosphere*. Cambridge University Press, pp 65–120
- Fahey DW, Schumann U (1999) “Aviation-produced aerosols and cloudiness,” in Intergovernmental Panel on Climate Change Special Report on Aviation and the Global Atmosphere, eds J. E. Penner, D. H. Lister, D. J. Griggs, D. J. Dokken, and M. McFarland (Cambridge: Cambridge University Press), 65–120
- Flynn CJ, Albert MYZ, Savyasachee M (2007) Novel polarization-sensitive micropulse lidar measurement technique. *Opt Express* 15(6):2785
- Forster P, Ramaswamy V, Artaxo P, Bernsten T, Betts R, Fahey DW, Haywood J, Lean J, Lowe DC, Myhre G (2007) Changes in atmospheric constituents and in radiative forcing. Chapter 2, in: *Climate Change 2007. The Physical Science Basis*
- Fortuin JPF, Becker CR, Fujiwar M, Immler F, Kelder HM, Scheele MP, Schrems O, Verver GHL (2007) Origin and transport of tropical cirrus clouds observed over Paramaribo, Suriname (5.8 N, 55.2 W). *J Geophys Res Atmos* 112
- Fu Q, Liou KN (1993) Parameterization of the radiative properties of cirrus clouds. *J Atmos Sci* 50(13):2008–2025
- Fu Q, Hu Y, Yang Q (2007) Identifying the top of the tropical tropopause layer from vertical mass flux analysis and CALIPSO lidar cloud observations. *Geophys Res Lett* 34(14). <https://doi.org/10.1029/2007GL030099>
- Hansen J, Sato M, Ruedy R, Lacis A, Asamoah K, Beckford K, Borenstein S, Brown E, Cairns B, Carlson B, Curran B, De Castro S, Druryan L, Etwarrow P, Ferde T, Fox M, Gaffen D, Glascoe J, Gordon H et al (1997) Forcings and chaos in inter-annual to decadal climate change. *J Geophys Res Atmos* 102. <https://doi.org/10.1029/97jd01495>
- Hartmann DL, Ockert-Bell ME, Michelsen ML (1992) The effect of cloud type on Earth's energy balance: global analysis. *J Clim* 5(11):1281–1304
- He QS, Li CC, Ma JZ, Wang HQ, Shi GM, Liang ZR, Luan Q, Geng FH, Zhou XW (2013) The properties and formation of cirrus clouds over the Tibetan Plateau based on summertime lidar measurements. *J Atmos Sci* 70(3):901–915
- Heidinger AK, Li Y, Baum BA, Holz RE, Platnick S, Yang P (2015) Retrieval of cirrus cloud optical depth under day and night conditions from MODIS collection 6 cloud property data. *Remote Sens*:7257–7271. <https://doi.org/10.3390/rs70607257>
- Heymsfield AJ, Miloshevich LM (1995) Relative humidity and temperature influences on cirrus formation and evolution: observations from wave clouds and FIRE II. *J Atmos Sci* 52:4302–4326
- Heymsfield AJ, Iaquinta J (2000) Cirrus crystal terminal velocities. *J Atmos Sci* 57(7):916–938
- Heymsfield AJ, McFarquhar GM, Collins WD, Goldstein JA, Valero FP, Spinhirne J, Hart W, Pilewskie P (1998) Cloud properties leading to highly reflective tropical cirrus: interpretations from CEPEX, TOGA COARE, and Kwajalein, Marshall Islands. *J Geophys Res Atmos* 103(D8):8805–8812
- Immler F, Treffeisen R, Engelbart D, Krüger K, Schrems O, Immler F, Treffeisen R, Engelbart D, Krüger K, Cirrus OS (2007) Cirrus, contrails, and ice supersaturated regions in high pressure systems at northern mid latitudes To cite this version : HAL Id : hal-00303090
- Jakob C (2001) Cloud parametrization-progress, problems and prospects. In: *Proceedings of an ECMWF seminar on key issues in parametrization*. ECMWF, pp 327–338
- Jeffery CA, Austin PH (1997) Homogeneous nucleation of super cooled water: results from a new equation of state. *J Geophys Res* 102:25, 259–25,279
- Jensen E, Toon O, Vay S, Ovarlez J, May R, Bui T, Twohy C, Gandrud B, Pueschel R, Schumann U (2001) Prevalence of ice-supersaturated regions in the upper troposphere: implications for optically thin ice cloud formation. *J Geophys Res* 106:17253–17266
- Jensen EJ, Kinne S, Toon OB (1994) Tropical cirrus cloud radiative forcing: sensitivity studies. *Geophys Res Lett* 21(18):2023–2026
- Jensen EJ, Diskin G, Lawson RP, Lance S, Bui TP, Hlavka D, McGill M, Pfister L, Toon OB, Gao R (2013) Ice nucleation and dehydration in the tropical tropopause layer. *Proc Natl Acad Sci* 110(6):2041–2046
- Joseph PV, Raman PL (1966) Existence of low level westerly jet stream over peninsular India during July. *Ind J Meteor Geophys* 17:407–410
- Joseph PV, Sijikumar S (2004) Intraseasonal variability of the low-level jet stream of the asian summer monsoon. *J Clim*:1449–1458
- Kärcher B (2018) Formation and radiative forcing of contrail cirrus. *Nat Commun* 9:1–17. <https://doi.org/10.1038/s41467-018-04068-0>
- Koop T, Luo B, Tsias A, Peter T (2000) Water activity as the determinant for homogeneous ice. *Nature* 406:611–614. <https://doi.org/10.1038/35020537>
- Korolev A, Isaac G (2006) Relative humidity in liquid, mixed-phase, and ice clouds. *J Atmos Sci* 63:2865–2880
- Koteswaram P (1956) Easterly jet stream in the tropics. *Res Report Met Dept Univ Chicago* 1956:1–23
- Koteswaram P (1958) The easterly jet stream in the tropics. *Tellus* X1958:43–57
- Kox S, Bugliaro L, Ostler A (2014) Retrieval of cirrus cloud optical thickness and top altitude from geostationary remote sensing. *Atmos Meas Tech* 7:3233–3246. <https://doi.org/10.5194/amt-7-3233-2014>
- Krämer M, Schiller C, Afchine A, Bauer R, Gensch I, Mangold A, Schlicht S, Spelten N, Sitnikov N, Borrmann S, De Reus M (2009) Ice supersaturations and cirrus cloud crystal numbers. *Atmos Chem Phys* 9(11):3505–3522
- Lawson RP, Woods S, Jensen E, Erfani E, Gurganus C, Gallagher M (2019) A review of ice particle shapes in cirrus formed in situ and in anvils journal of geophysical research. *Atmospheres*:49–90. <https://doi.org/10.1029/2018JD030122>
- Liou KN (1986) Influence of cirrus clouds on weather and climate processes: a global perspective. *Mon Weather Rev* 114(6):1167–1199
- Liou K-N (2002) *An introduction to atmospheric radiation*. Elsevier
- Liou KN, Takano Y (2002) Interpretation of cirrus cloud polarization measurements from radiative transfer theory. *Geophys Res Lett* 29:1–4
- Lolli S, Welton EJ, Lewis JR, Campbell JR, Vivone G (2020) Features and characteristics of the new NASA MicroPuLse

- NETwork (MPLNET) automatic rain detection algorithm. IOP Conf Ser: Earth Environ Sci 489(1):012028
- Lynch DK (1996) Cirrus clouds: their role in climate and global change. *Acta Astronaut* 38:859–863. [https://doi.org/10.1016/S0094-5765\(96\)00098-7](https://doi.org/10.1016/S0094-5765(96)00098-7)
- Lynch DK (2000) Cirrus, ice crystals and halos. *Optics & Photonics News* 11(1):32
- Manoj Kumar N, Venkatramanan K (2020) Lidar observed optical properties of tropical Cirrus clouds over Gadanki region. *Front Earth Sci* 8:140
- Manoj Kumar N, Venkatramanan K, Nair AK, Sathesh Kumar S (2020) On the characterization of descending nature of cirrus clouds over a tropical site, Gadanki. *Int J Remote Sens* 41(17):6550–6569
- Mbatha N, Shikwambana L (2022) First observations of cirrus clouds using the UZ Mie Lidar over uMhlathuze City, South Africa. *Appl Sci* 12(9):4631
- McFarquhar GM, Heymsfield AJ, Spinhirne J, Hart B (2000) Thin and subvisual tropopause tropical cirrus: observations and radiative impacts. *J Atmos Sci* 57(12):1841–1853
- Meenu S, Rajeev K, Parameswaran K (2011) Regional and vertical distribution of semitransparent cirrus clouds over the tropical Indian region derived from CALIPSO data. *J Atmos Solar-Terrestrial Phys* 73:1967–1979. <https://doi.org/10.1016/j.jastp.2011.06.007>
- Mitchell DL, Rasch P, Ivanova D, McFarquhar G, Nousiainen T (2008) Impact of small ice crystal assumptions on ice sedimentation rates in cirrus clouds and GCM simulations. *Geophys Res Lett* 35(9)
- Müller D, Tesche M, Eichler H, Engelmann R, Althausen D, Ansmann A, Cheng YF, Zhang YH, Hu M (2006) Strong particle light absorption over the Pearl River Delta (South China) and Beijing (North China) determined from combined Raman lidar and sun photometer observations. *Geophys Res Lett* 33(20)
- Müller D, Ansmann A, Mattis I, Tesche M, Wandinger U, Althausen D, Pisani G (2007) Aerosol-type-dependent lidar ratios observed with Raman lidar. *J Geophys Res Atmos* 112(D16)
- Muri H, Kristjánsson JE, Storelvmo T, Pfeffer MA (2014) The climatic effects of modifying cirrus clouds in a climate engineering framework. *J Geophys Res* 119:4174–4191. <https://doi.org/10.1002/2013JD021063>
- Nair AKM, Rajeev K, Mishra MK, Thampi BV (2012) Multiyear lidar observations of the descending nature of tropical cirrus clouds. *J Geophys Res* 117:1–9. <https://doi.org/10.1029/2011JGD017406>
- Nicolas JP, Bromwich DH (2011) Climate of West Antarctica and influence of marine air intrusions. *J Clim* 24:49–67
- Noel V, Chepfer H, Haeffelin M, Morille Y (2006) Classification of ice crystal shapes in midlatitude ice clouds from three years of lidar observations over the SIRTa observatory. *J Atmos Sci* 63(11):2978–2991
- Pandit AK, Gadhavi HS, Ratnam MV, Raghunath K, Rao SVB, Jayaraman A (2015) Long-term trend analysis and climatology of tropical cirrus clouds using 16 years of lidar data set over Southern India. *Atmos Chem Phys*:13833–13848. <https://doi.org/10.5194/acp-15-13833-2015>
- Pfister L, Selkirk HB, Jensen EJ, Schoeberl MR, Toon OB, Browell EV, Grant WB, Gary B, Mahoney MJ, Bui TV, Hintsa E (2001) Aircraft observations of thin cirrus clouds near the tropical tropopause. *J Geophys Res Atmos* 106(D9):9765–9786
- Podglajen A, Plougonven R, Hertzog A, Legras B (2015) Large scale and cloud scale dynamics and microphysics in the formation and evolution of a TTL cirrus : a case modelling study. *Atmos Chem Phys* 17:9789
- Prabhakara C, Kratz DP, Yoo JM, Dalu G, Vernekar A (1993) Optically thin cirrus clouds: radiative impact on the warm pool. *J Quant Spectrosc Radiat Transf* 49:467–483. [https://doi.org/10.1016/0022-4073\(93\)90061-L](https://doi.org/10.1016/0022-4073(93)90061-L)
- Rajeev K, Parameswaran K, Thampi BV, Mishra MK, Nair AK, Meenu S (2010) Altitude distribution of aerosols over south-east Arabian Sea coast during pre-monsoon season: elevated layers, long-range transport and atmospheric radiative heating. *Atmos Environ* 44(21–22):2597–2604
- Ramanathan V, Collins W (1991) Thermodynamic regulation of ocean warming by cirrus clouds deduced from observations of the 1987 El Nino. *Nature* 351(6321):27–32
- Ramaswamy T (2006) Micropulse lidar observations of free tropospheric aerosols over the atmospheric radiation measurement site at Barrow. Thesis, The University of Alaska Fairbanks, Alaska
- Saha S, Niranjana Kumar K, Sharma S, Kumar P, Joshi V (2020) Can Quasi-Periodic Gravity Waves influence the shape of ice crystals in cirrus clouds? *Geophys Res Lett* 47(11):e2020GL087909
- Saha S, Sharma S, Kumar KN, Kumar P, Joshi V, Georgoussis G, Lal S (2021) A case study on the vertical distribution and characteristics of aerosols using ground-based raman lidar, satellite and model over Western India. *Int J Remote Sens* 42(17):6417–6432
- Saseen K, Cambell JR (2001) A mid-latitude cirrus cloud climatology from the facility for atmospheric remote sensing: part I. Microphysical and synoptic properties. *J Atmos Sci* 58:481–496
- Sassen K, Wang L, Starr DOC, Comstock JM, Quante M (2007) A midlatitude cirrus cloud climatology from the facility for atmospheric remote sensing. Part V: Cloud structural properties. *J Atmos Sci* 64:2483–2501. <https://doi.org/10.1175/JAS3949.1>
- Sassen K, Wang Z, Liu D (2009) Global distribution of cirrus clouds from CloudSat/Cloud-Aerosol Lidar and infrared pathfinder satellite observations (CALIPSO) measurements. *J Geophys Res Atmos* 114:1–12. <https://doi.org/10.1029/2008JD009972>
- Sassen K, Wang Z, Liu D (2009) Cirrus clouds and deep convection in the tropics : Insights from CALIPSO and CloudSat. *J Geophys Res* 114:1–11. <https://doi.org/10.1029/2009JD011916>
- Sathesh SK, Vinoj V, Moorthy KK (2006) Vertical distribution of aerosols over an urban continental site in India inferred using a micro pulse lidar. *Geophys Res Lett* 33(20)
- Schumann U (2002) Contrail cirrus. *Cirrus*:231–255
- Schumann U, Bugliaro L, Dörnbrack A, Baumann R, Voigt C (2021) Aviation contrail cirrus and radiative forcing over europe during 6 months of COVID-19. *Geophys Res Lett* 48. <https://doi.org/10.1029/2021GL092771>
- Seifert P, Ansmann A, Mu D, Wandinger U, Althausen D, Heymsfield AJ (2007) Cirrus optical properties observed with lidar, radiosonde, and satellite over the tropical Indian Ocean during the aerosol-polluted northeast and clean maritime southwest monsoon. *J Geophys Res* 112:1–14. <https://doi.org/10.1029/2006JD008352>
- Sharma S, Vaishnav R, Shukla MV, Kumar P, Kumar P, Thapliyal PK, Lal S, Acharya YB (2016) Evaluation of cloud base height measurements from ceilometer CL31 and MODIS satellite over Ahmedabad, India. *Atmos Meas Tech* 9(2):711–719
- Shine KP (1994) Panel discussion on putting solar variability in perspective. In: Nesme-Ribes E (ed) *The solar engine and its influence on terrestrial atmosphere and climate*. Springer, Berlin Heidelberg, Berlin, Heidelberg, pp 369–380
- Sivakumar V, Bhavanikumar Y, Rao PB, Mizutani K, Aoki T, Yasui M, Itabe T (2003) Lidar observed characteristics of the tropical cirrus clouds. *Radio Sci* 38:1094
- Solomon SD, Qin M, Manning M, Marquis K, Averyt MMB, Tignor HL, Miller Jr, Chen (2007) *Climate change*. In: *The physical science basis*. Cambridge University Press, 996 pp

- Spinhirne JD (1993) Micro pulse lidar. *IEEE Trans Geosci Remote Sens* 31:48–55. <https://doi.org/10.1109/36.210443>
- Stephens GL, Webster PJ (1981) Clouds and climate: sensitivity of simple systems. *J Atmos Sci* 38:235–247
- Stocker TF, Qin D, Plattner GK, Tignor M, Allen SK, Boschung J, Nauels A, Xia Y, Bex B, Midgley BM (2013) Climate change 2013: The physical science basis. In: Contribution of working group I to the fifth assessment report of the intergovernmental panel on climate change. Cambridge University Press, Cambridge; New York, p 1535
- Stubenrauch CJ, Cros S, Guignard A, Lamquin N (2010) A 6-year global cloud climatology from the Atmospheric InfraRed Sounder AIRS and a statistical analysis in synergy with CALIPSO and CloudSat. *Atmos Chem Phys* 10(15):7197–7214
- Stubenrauch CJ, Rossow WB, Kinne S, Ackerman S, Cesana G, Chepfer H, Di Girolamo L, Getzewich B, Guignard A, Heidinger A, Maddux BC, Menzel WP, Minnis P, Pearl C, Platnick S, Poulsen C, Riedi J, Sun-Mack S, Walther A, Winker D, Zeng S, Zhao G (2013) Assessment of global cloud datasets from satellites: project and database initiated by the GEWEX radiation panel. *Bull Am Meteorol Soc* 94:1031–1049. <https://doi.org/10.1175/BAMS-D-12-00117.1>
- Sunilkumar SV, Parameswaran K (2005) Temperature dependence of tropical cirrus properties and radiative effects. *J Geophys Res Atmos* 110(D13)
- Sunilkumar SV, Parameswaran K, Rajeev K, Murthy BK, Meenu S, Mehta SK, Babu A (2010) Semitransparent cirrus clouds in the tropical tropopause layer during two contrasting seasons. *J Atmos Sol Terr Phys* 72(9–10):745–762
- Takano Y, Liou KN (1995) Radiative transfer in cirrus clouds. Part III: light scattering by irregular ice crystals. *J Atmos Sci*. [https://doi.org/10.1175/1520-0469\(1995\)052%3c0818:RTICCP%3e2.0.CO;2](https://doi.org/10.1175/1520-0469(1995)052%3c0818:RTICCP%3e2.0.CO;2)
- Taylor JR, Randel WJ, Jensen EJ (2011) Cirrus cloud-temperature interactions in the tropical tropopause layer: a case study. *Atmos Chem Phys* 11(19):10085–10095
- Uchino O, Tabata I, Kai K, Okada Y (1988) Polarization properties of middle and high level clouds observed by lidar. *J Meteorol Soc Jpn Ser II* 66(4):607–616
- Veerabuthiran S (2004) High-altitude cirrus clouds and climate. *Resonance* 9:23–32. <https://doi.org/10.1007/bf02834985>
- Wang W, Yi F, Liu F, Zhang Y, Yu C, Yin Z (2020) Characteristics and seasonal variations of cirrus clouds from polarization lidar observations at a 30 N plain site. *Remote Sens* 12(23):3998
- Welton EJ, Campbell JR (2002) Micropulse lidar signals: uncertainty analysis. *J Atmos Ocean Technol* 19(12):2089–2094
- Wylie D, Piironen P, Wolf W, Eloranta E (1995) Understanding satellite cirrus cloud climatologies with calibrated lidar optical depths. *J Atmos Sci* 52(23):4327–4343
- Xie H, Zhou T, Fu Q, Huang J, Huang Z, Bi J, Shi J, Zhang B, Ge J (2017) Automated detection of cloud and aerosol features with SACOL micro-pulse lidar in northwest China. *Opt Express* 25(24):30732–30753
- Zeng X, Gong J, Li X, Wu DL (2021) Modeling the radiative effect on microphysics in cirrus clouds against satellite observations. *J Geophys Res Atmos* 126:1–21. <https://doi.org/10.1029/2020JD033923>
- Zerefos CS, Eleftheratos K, Balis DS, Zanis P, Tselioudis G, Meleti C (2003) Evidence of impact of aviation on cirrus cloud formation. *Atmos Chem Phys* 3(5):1633–1644

Publisher's note Springer Nature remains neutral with regard to jurisdictional claims in published maps and institutional affiliations.

Springer Nature or its licensor (e.g. a society or other partner) holds exclusive rights to this article under a publishing agreement with the author(s) or other rightsholder(s); author self-archiving of the accepted manuscript version of this article is solely governed by the terms of such publishing agreement and applicable law.